Large efficiency improvements in BEAMnrc using directional bremsstrahlung splitting

I. Kawrakow, D. W. O. Rogers,[a)] and B. R. B. Walters[b)]
Ionizing Radiation Standards, National Research Council of Canada, Ottawa K1A OR6, Canada

(Received 18 February 2004; revised 28 June 2004; accepted for publication 12 July 2004; published 1 October 2204)

The introduction into the BEAMnrc code of a new variance reduction technique, called directional bremsstrahlung splitting (DBS), is described. DBS uses a combination of interaction splitting for bremsstrahlung, annihilation, Compton scattering, pair production and photoabsorption, and Russian Roulette to achieve a much better efficiency of photon beam treatment head simulations compared to the splitting techniques already available in BEAMnrc (selective bremsstrahlung splitting, SBS, and uniform bremsstrahlung splitting, UBS). In a simulated 6 MV photon beam (10×10 cm^2 field) photon fluence efficiency in the beam using DBS is over 8 times higher than with optimized SBS and over 20 times higher than with UBS, with a similar improvement in electron fluence efficiency in the beam. Total dose efficiency in a central-axis depth-dose curve improves by a factor of 6.4 over SBS at all depths in the phantom. The performance of DBS depends on the details of the accelerator being simulated. At higher energies, the relative improvement in efficiency due to DBS decreases somewhat, but is still a factor of 3.5 improvement over SBS for total dose efficiency using DBS in a simulated 18 MV photon beam. Increasing the field size of the simulated 6 MV beam to 40×40 cm^2 (broad beam) causes the relative efficiency improvement of DBS to decrease by a factor of $\approx$1.7 but is still up to 7 times more efficient than with SBS. *© 2004 American Association of Physicists in Medicine.* [DOI: 10.1118/1.1788912]

I. INTRODUCTION

BEAMnrc[1,2] is a widely-used Monte Carlo code for simulating radiotherapy beams (see Ref. 3 for a listing of over 150 publications). In the simulation of photon beams, a variance reduction technique that is often used involves "splitting" bremsstrahlung interactions, so that each bremsstrahlung event produces NBRSPL photons each having weight NBRSPL^{-1}, where NBRSPL is the bremsstrahlung splitting number that is controlled by the user. bremsstrahlung splitting can greatly decrease the uncertainty in all photon quantities (e.g., dose due to photons, photon fluence, photon energy spectrum) at the bottom of the accelerator for a given number of electrons incident on the photon target. The decrease in uncertainty is greater than the increase in CPU time/history required by bremsstrahlung splitting, so the overall result is an increased efficiency in photon quantities at the bottom of the accelerator. In the original version of BEAM there was an option to use uniform bremsstrahlung splitting (UBS). In 1998 an improved splitting routine, selective bremsstrahlung splitting (SBS), was added to the code and further enhanced the efficiency.[4,5] In this paper we report a further significant improvement in efficiency from an algorithm called directional bremsstrahlung splitting (DBS). We describe a specific implementation in the BEAMnrc system (which has been made available with the BEAMnrc04 release) but the techniques described are applicable in general and could be used to improve the efficiency of any Monte Carlo code for simulating photon accelerators.

II. UNIFORM AND SELECTIVE BREMSSTRAHLUNG SPLITTING

In UBS, NBRSPL is set to a constant user-input value (usually between 20 and 100). On the other hand, SBS varies the value of NBRSPL to maximize splitting of photons aimed into the field and minimize unnecessary splitting of photons aimed away from the field. The value of NBRSPL for a bremsstrahlung event is based on the energy and direction of the incident electron and is proportional to the integrated probability of the bremsstrahlung photon entering a user-defined field [defined by field size, FS (width of a square field) and SSD, usually at the bottom of the accelerator]. SBS also requires the user to set a lower limit on NBRSPL, called the background splitting number. Several guidelines are suggested[2] for the use of SBS, such as selection of a maximum splitting number between 200 and 1000, with a background splitting number equal to one-tenth of the maximum, and selection of a field size which is 10 cm greater than the actual field width.

If the user is not interested in electron statistics at the bottom of the accelerator, then both UBS and SBS offer the option of playing Russian Roulette with all secondary and higher-order charged particles. This entails setting a survival probability threshold equal to NBRSPL^{-1} for each secondary/higher-order charged particle and comparing this threshold to a random number. If the random number is higher than the survival threshold, then the charged particle is eliminated immediately after it has been created. If the random number is less than or equal to the survival threshold, then the charged particle is kept, and its weight is increased by a factor of NBRSPL. This higher-weight particle carries the transport physics for itself and all of the secondary/higher-order charged particles that were eliminated by Russian Roulette. Russian Roulette can increase the efficiency of UBS and SBS by a factor of 2, however, as mentioned above, the electron statistics will be compromised.

If Russian Roulette is turned on, then both UBS and SBS will split higher-order bremsstrahlung photons and photons from annihilation events (in either case, these will be photons created by higher-weight charged particles that have survived Russian Roulette). In UBS, the splitting number for these events is equal to that used for primary bremsstrahlung events. In SBS, the splitting number for these higher-order events is equal to the background splitting number for primary bremsstrahlung events. If Russian Roulette is off, then UBS and SBS do not split higher-order bremsstrahlung or annihilation events to avoid spending CPU time tracking particles of vanishing weight.

Both UBS and SBS have limitations. As mentioned above, the nondirectional nature of UBS means that much of the CPU time is spent tracking split photons that will not make it to the field of interest at the bottom of the accelerator. While SBS is intended to remedy this by maximizing the splitting of those photons aimed into the field of interest, statistics in the field of interest are compromised by the large range of photon weights that result from having a variable splitting number. In addition, SBS requires additional CPU time for "background splitting" of bremsstrahlung photons aimed away from the field. Background splitting was found to be necessary to prevent high-weight photons from "chance events" (e.g., photons incorrectly deemed out of the field of interest by the selective splitting function, or photons initially aimed away from the field and then scattering back into it) from compromising the statistics in the field of interest.

III. DIRECTIONAL BREMSSTRAHLUNG SPLITTING

We are introducing another bremsstrahlung splitting routine called directional bremsstrahlung splitting (DBS) into the BEAMnrc code. It is designed to overcome the limitations of SBS, by ensuring that all photons in the field of interest have the same weight and by eliminating the need for "background splitting."

Similar to SBS, DBS requires the user to define a field of interest (using the field radius and the SSD). Beyond this, however, the two algorithms diverge. The complete DBS algorithm is fairly complex. In Secs. III A–III G we present details of the algorithm that leads to a large increase in the efficiency calculating the photon fluence but leads to poor statistics for contaminant electrons. The full algorithm, including improved statistics for electron contamination, is presented in Sec. III H.

A. Bremsstrahlung events

In general, bremsstrahlung events initiated by a primary, or by a fat (high-weight) electron (more about fat electrons below) are split by a fixed, user-defined splitting number, NBRSPL, with the resultant photons all having weight NBRSPL^{-1}. The algorithm then loops through all NBRSPL split photons and, for each one, determines whether or not it is aimed into the field of interest. If it is, then the photon is kept. If not, then Russian Roulette is played on the photon by comparing a random number to a survival threshold of NBRSPL^{-1}. If the random number is less than this number, then the photon is kept and its weight is increased by a factor of NBRSPL. Photons aimed away from the field of interest which survive this Russian Roulette are fat and all have the same weight (normally unity).

If the user has set the EGSnrc parameters in BEAMnrc to only use the leading term of the Koch–Motz distribution for determining bremsstrahlung angles[6,7] (the default in BEAMnrc), then, rather than loop through NBRSPL bremsstrahlung interactions, DBS saves further CPU time by invoking a subroutine called do_smart_brems. This subroutine determines how many of the NBRSPL split photons will be aimed into the field before the bremsstrahlung event is simulated and only generates those photons. It also samples an angle from the full distribution and, if the direction is not aimed at the field, a single fat bremsstrahlung photon travelling in this direction is generated. This fat photon is equivalent to a photon that has survived Russian Roulette in the general DBS treatment of bremsstrahlung events. Details of the equations used in the implementation of do_smart_brems are given in Appendix A. This is a proper variance reduction technique which does not bias the physics of the simulation.

B. Annihilation events

If a primary, or if a fat positron (more about fat positrons below) undergoes an annihilation event, then DBS splits the event by NBRSPL, the same user-defined splitting number used to split bremsstrahlung events. Resultant photons all have weight NBRSPL^{-1} and, similar to bremsstrahlung splitting, the code then loops through the NBRSPL resultant photons and plays Russian Roulette with those not aimed into the field of interest. Photons which survive Russian Roulette have their weight increased (i.e., they become fat). If the positron is at rest when it annihilates, DBS uses a subroutine called uniform_photons to generate the split photons. The algorithm is similar to the algorithm of do_smart_brems described in Appendix A, except that the probability W' is simply given by $(\mu_{\max}-\mu_{\min})/2$ and the sampling of directions is done uniformly between $\mu_{\min}$ and $\mu_{\max}$.

C. Compton events

The treatment of Compton events by DBS depends on whether the photon about to undergo the Compton event is fat (i.e., has survived Russian Roulette) or not.

If a nonfat photon is about to undergo a Compton event then (1) if the event is about to take place in a gas (any material with $\rho \leqslant 0.012\ \mathrm{g/cm^3}$), then DBS allows the single Compton event to proceed normally and plays Russian Roulette with the resultant Compton scattered photon if it is not aimed into the field of interest. (2) Otherwise, DBS plays Russian Roulette with the photon before the event can take place. If this photon survives, then its weight is increased by a factor of NBRSPL and it becomes fat. The special treatment of the in-gas case is to prevent possible creation of fat photons immediately above the field of interest which could, in turn create a large number of nonfat photons which enter the phantom with similar characteristics.

If the photon about to undergo a Compton event is fat (either because it was fat to begin with or because it started as nonfat, but survived the Russian Roulette described above), then DBS splits the Compton event NBRSPL times. Generally, splitting the Compton event entails calling the EGSnrc subroutine COMPT NBRSPL times, with all resulting particles having weight NBRSPL^{-1} times the weight of the fat photon undergoing the event. Then, DBS loops through all resultant particles, performing Russian Roulette on any Compton scattered photons not directed into the field of interest and on all secondary electrons (including from Auger and/or Coster-Kronig events). As always, particles that survive Russian Roulette have their weight increased by a factor of NBRSPL, thereby becoming fat.

If the EGSnrc bound Compton scattering option is off (i.e., the Klein–Nishina approximation, which is the BEAMnrc default, is being used), then, instead of the general Compton splitting algorithm outlined above, DBS saves CPU time by using a subroutine called do_smart_compton. In a similar way as do_smart_brems, this subroutine calculates how many of the NBRSPL Compton scattered photons will have a polar angle that can direct them into the field of interest and only generates these. In addition, do_smart_compton generates a single Compton scattered photon with no angular restrictions. If this photon happens to be directed outside the field of interest, then it is kept as a fat photon with weight 1, and carries the physics for all photons not directed into the field. On the other hand, if the photon happens to be directed into the field of interest it is unnecessary (since all of these photons have already been generated) and is discarded immediately. Finally, do_smart_compton creates a single fat electron of weight equal to the weight of the original fat photon undergoing the Compton event. More details about the equations and sampling algorithm used are given in Appendix B.

D. Pair production events

Similar to Compton events, if a nonfat photon is about to undergo a pair production event, then DBS only allows the event to take place if the photon is about to interact in a gas. Otherwise, DBS plays Russian Roulette with the photon. If the photon survives, it becomes fat, with its weight increased by a factor of NBRSPL and then undergoes the pair production event.

A fat photon is always allowed to undergo a pair production event, but the event is not split (unlike Compton). This ensures that the resultant charged particle pair will be fat (except in a gas).

E. Photoelectric events

Photoelectric events are treated the same as pair production events. This ensures that all photoelectrons are fat (except in a gas).

F. Fluorescent photons

After a photoelectric event, a fluorescent photon may be created. If the fluorescent photon is nonfat (from a photoelectric event undergone by a nonfat photon), then it is subject to Russian Roulette if not directed into the field of interest. If the fluorescent photon is fat (from a photoelectric event undergone by a fat photon), DBS splits it NBRSPL times isotropically using the uniform_photons subroutine described in the section on annihilation events above. This ensures that any fluorescent photon reaching the field of interest is nonfat.

G. Summary of DBS without electron splitting

In summary, the techniques described up to this point ensure that all photons inside the circular target field will be nonfat, i.e., have a weight of 1/NBRSPL and those outside it will have a weight 1. If the splitting number NBRSPL is large, there will be very few fat photons that do not reach the field of interest compared to the many low-weight photons that do. Therefore only very little time will be spent transporting photons that do not contribute to the fluence in the field of interest. Similarly, all electrons will be fat except for those few created by nonfat photons interacting in the air just above where the phase-space file is created. As a result, a very small fraction of the CPU time will be spent transporting electrons.

H. Electron splitting

As described up to this point, the DBS technique eliminates electrons generated by split particles/interactions, either by playing Russian Roulette with them or by not generating them at all. The result is that electrons are represented by relatively few fat particles reaching the bottom of the accelerator, and therefore the contaminant electron statistics are poor. In most practical applications, one is interested in the contribution of electrons to the total dose. In order to improve the statistics of electrons, a few modifications to the DBS technique described so far are necessary.

Generally, the further away from the bottom of the accelerator the electrons are produced, the smaller their chance to reach the patient plane. In particular, primary electrons and electrons set in motion in the photon target and primary collimator virtually never arrive at the bottom of the accelerator. On the other hand, electrons set in motion in the lower portion of the flattening filter and close to the inner and lower edges of the photon jaws, have a relatively high chance of reaching the patient plane. Given these observations, the strategy for improving the statistics of contaminant electrons is clear: (i) spend as little time as possible transporting electrons in the upper portion of the treatment head, i.e., use DBS as described above, and (ii) increase the number of transported electrons in the lower part of the treatment head by using electron splitting and turning off Russian Roulette played before photon interactions. We will refer to these modifications as "DBS with electron splitting" in what follows.

When electron splitting is turned on, the user defines two planes perpendicular to the beam axis: the splitting plane, and the Russian Roulette plane, where the Russian Roulette plane is above the splitting plane. These two planes divide the treatment head in three distinct parts.

(1) An "upper" portion (above the Russian Roulette plane), where DBS is used as described above with the result of very few fat electrons being transported.
(2) A "lower" portion (below the splitting plane), where the goal is to have many low-weight electrons and no fat electrons.
(3) A transitional region (between the splitting and Russian Roulette planes), where there is a mixture of fat and low-weight electrons.

The splitting plane is defined by specifying one of the BEAMnrc component modules (CMs) in the simulation and selecting an existing plane (i.e., a boundary between layers or at the top or bottom of the CM) within the CM. Usually the CM specified for the splitting plane is the flattening filter, and the plane selected is close to the bottom of the filter. Fat electrons crossing the splitting plane are split NBRSPL times (and have their weight reduced by a factor of NBRSPL). There is also an option to redistribute the split electrons assuming radial symmetry about the beam axis. In most cases this improves the spatial distribution of electrons when the beam is radially symmetric above this plane.

The Russian Roulette plane is defined by specifying its z position. It is usually above the splitting plane but still within the flattening filter CM. Below the Russian Roulette plane, the following modifications are applied to the DBS algorithm to maximize production of low-weight electrons:

(1) Low-weight photons about to undergo pair production, Compton, or photoelectric events are allowed to interact normally. However, scattered or fluorescent photons resulting from such interactions are subjected to Russian Roulette with a probability NBRSPL^{-1}, if they do not go towards the field of interest.
(2) If a fat photon undergoes a pair production or photoelectric event, the event is split NBRSPL times to generate NBRSPL (photoabsorption) or $2\times$NBRSPL (pair production) low-weight charged particles.
(3) If a fat photon undergoes a Compton event then the event is split NBRSPL times and Russian Roulette is not played with any resultant charged particles. The subroutine do_smart_compton is never used. The NBRSPL scattered photons originating from such split Compton events are subjected to Russian Roulette, if they do not go towards the field of interest.

Note that the nonfat charged particles generated by the electron splitting algorithm described above may, in turn, generate nonfat photons through bremsstrahlung or annihilation events. These photons are subject to Russian Roulette if they are not directed into the field of interest.

Electron splitting ensures an increase in the number of electrons in the field at a cost in the CPU time required to transport them. At the same time, all photons going towards the field of interest are still low-weight and all photons directed away from the field of interest are fat.

IV. PERFORMANCE OF DIRECTIONAL BREMSSTRAHLUNG SPLITTING

All of the techniques applied in DBS are standard variance reduction techniques (splitting, Russian Roulette, biased sampling) and thus they do not change the physics of the calculation and they provide an unbiased estimate of any scored quantity.[8] To ensure that we had not introduced any bugs into the coding, we made sure that the results obtained with and without the DBS algorithm were identical within good statistics for all of the efficiency tests discussed in the following and for a variety of other situations as well. Once the accuracy is established, it is critical to measure the improvement in efficiency for a variety of situations since variance techniques are not guaranteed to improve efficiency, just to maintain accurate physics.

In order to look at the performance of DBS, we used BEAMnrc to do a full simulation of a 6 MV photon beam from an Elekta SL25 accelerator (10×10 cm^2 field at the phantom surface at SSD$=$100 cm) and examined fluence at the SSD and dose in a water phantom placed at the bottom of the accelerator.

Apart from the bremsstrahlung splitting parameters, simulation parameters were identical to those used by Sheikh-Bagheri and Rogers.[9,10] In particular, range rejection was performed on charged particles with energies <2 MeV, with rejection occurring if the particle did not have sufficient energy to make it to the nearest region boundary. The jaws defining the field were modelled after jaws that are intended to be used with a multileaf collimator attachment. These jaws differed from standard jaws (which are 10 cm thick, comprising 5 cm of tungsten and 5 cm of lead, in both X and Y directions) in that they consisted only of tungsten with thickness 3 cm in the Y direction and 8 cm in the X direction. Thus, these jaws resulted in greater photon fluence outside the field, especially in the Y direction, than the standard jaws.

In all the cases presented below, performance of a bremsstrahlung splitting algorithm is specified by the efficiency, ϵ, given by

$$\epsilon = \frac{1}{s^2 T}, \tag{1}$$

where s is an estimate of the uncertainty on the quantity of interest (e.g., fluence or dose) and T is the CPU time required to achieve this uncertainty.

Uncertainty was evaluated using the history-by-history method[11] which takes into account correlations between contributions to fluence or dose from particles which arise from the same initial history. This is essential when using the splitting techniques described here since each initial electron may give rise to many split photons and electrons, each contributing to the same scored quantity. Failure to take into account these correlations can result in an underestimate of the uncertainty.

A. Fluence scoring

In a treatment head simulation that does not use variance reduction techniques, the uncertainty on the photon fluence within the beam for a given number of incident particles will be proportional to the inverse of the scoring zone area. The efficiency will therefore decrease with decreasing scoring zone area but the efficiency divided by the scoring zone area will be a constant. This is not necessarily the case in simulations where variance reduction techniques such as bremsstrahlung splitting are used. The smaller the scoring zone is, the smaller the probability will be that two or more particles that result from the same incident electron history will reach the zone. Ultimately, if the scoring zones are made infinitely small, correlations between particles from the same history will become negligible (the scoring zone is either reached by a single particle or not reached at all, this is the same as when no splitting was applied). Correlations between particles from the same incident electron history will modify the uncertainty compared to a situation where the same number of particles reaches the scoring plane but all particles are statistically independent. Depending on the nature of the correlation, the uncertainty may increase or decrease.

Given the above observations, one should score quantities such as dose or fluence in scoring zones of size that is relevant for treatment planning applications (i.e., squares or cubes of 5 mm or less) in order to be able to reliably assess the performance of a particular variance reduction technique. Unfortunately, BEAMnrc simulations without any variance reduction techniques used (which is our baseline) take a prohibitively long time to obtain reasonable statistical uncertainty in such small voxels. We have therefore selected slightly larger scoring zone sizes: 41×41 1×1 cm^2 scoring zones for the photon fluence and 21×11 2×4 cm^2 scoring zones for the electron fluence in a plane perpendicular to the beam axis at SSD$=$100 cm.

To assess the influence of the selected scoring zone size on the efficiency of the various splitting techniques relative to using no splitting, we varied the size of the central-axis fluence scoring zone for simulations performed with typical optimized parameters (see Sec. IV B for discussion of parameter selection). Figure 1 presents these results of relative photon fluence efficiencies. Each curve has been divided by the numbers shown in the figure (50.6, 11.5, and 7.37) to emphasize the shape of each curve [and to normalize the values for the 6×6 cm^2 scoring zone to 1.00]. One must note that we are presenting the relative efficiencies, and that for the no-splitting case, the absolute efficiency decreases almost exactly proportionally to the area of the scoring zone. However, it is clear that this is not the case for the bremsstrahlung splitting routines and that in particular the efficiency of the DBS algorithm decreases by almost an order of magnitude less going from the largest to smallest scoring zone sizes and thus the relative efficiency increases. The crucial point that Fig. 1 demonstrates is that the decrease of correlations with decreasing scoring zone size implies that the relative efficiency for DBS goes up substantially more than for UBS or SBS as the scoring region decreases in size. It is therefore clear that DBS will perform better relative to SBS or UBS when using scoring zone sizes typical for dose calculations in modern radiotherapy treatment planning (5 mm or less) and therefore the DBS efficiency results presented here represent a lower bound on the improvement in simulation efficiency in practical calculations. A rigorous explanation of the behavior observed in Fig. 1 has been found and will be presented elsewhere.

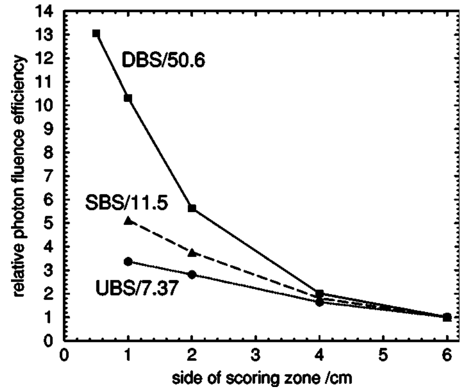

FIG. 1. Photon fluence efficiency for the three bremsstrahlung splitting techniques (DBS, directional, SBS, selective and UBS, uniform bremsstrahlung splitting) relative to that for no splitting as a function of the side of the square scoring region on the central axis. An Elekta SL25 6 MV 10×10 cm^2 photon beam is simulated. To emphasize the shapes of the curves, the results are normalized to the relative efficiency for the 6×6 cm^2 scoring zone size in each case by dividing the results by the values shown in the figure. The relative efficiency is a strong function of the size of the scoring region, the relative improvement increasing as the scoring area decreases (although the absolute efficiency decreases with the area of the scoring region for the no-splitting case).

Throughout this paper, results are presented relative to the efficiency for the baseline calculation with no splitting being used. This baseline efficiency varies quite dramatically, generally with a shape corresponding to the dose or fluence profile of interest. For example, the efficiency outside the beam is much lower because of the reduced number of photons involved.

B. Selecting splitting parameters

Setting of splitting parameters for each of the bremsstrahlung splitting routines was heavily weighted towards optimizing photon fluence efficiency, since photons were the greatest contributors to fluence or dose in our modelled accelerator. However, we also examined electron fluence efficiency, and, in the case of DBS with electron splitting, took it into account when selecting the best position of the splitting and Russian Roulette planes.

Rather than examine the fluence efficiency in each scoring zone while setting parameters, we examined the total efficiency in all scoring zones completely contained within the 10×10 cm^2 field of the beam. In the case of photon fluence this would comprise 81 of the 1×1 cm^2 zones, and in the case of electron fluence 5 of the 2×4 cm^2 zones. The square of the uncertainty used in calculating total efficiency was simply equal to the sum of the squares of the absolute uncertainty in each of these scoring zones.

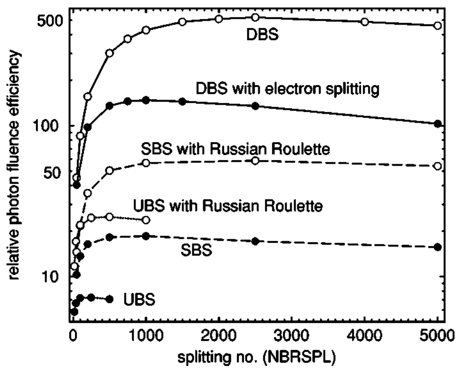

FIG. 2. Relative efficiency for calculating photon fluence within the 10×10 cm^2 field of a simulated Elekta SL25 6 MV photon beam as a function of bremsstrahlung splitting number (NBRSPL). Efficiencies shown are relative to total photon fluence efficiency with no splitting. For UBS and SBS, efficiencies are shown with Russian Roulette on (open circles) and off (solid circles). The field size parameter, FS, used with SBS was 30 cm (Refs. 9 and 10). For DBS, results are shown with electron splitting off (open circles) and electron splitting on with the splitting plane at $Z=15.46$ cm and the Russian Roulette plane at $Z=15.2$ cm (closed circles). For UBS the minimum splitting number is 20 and for SBS and DBS it is 50. Note the y axis is logarithmic.

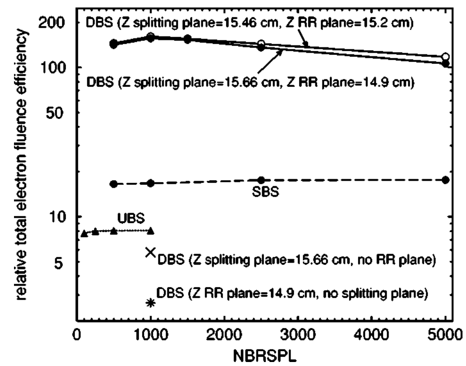

FIG. 3. Total electron fluence efficiency in the 10×10 cm^2 field of a simulated Elekta SL25 6 MV photon beam as a function of bremsstrahlung splitting number (NBRSPL). Efficiencies shown are relative to total electron fluence efficiency with no splitting. In the cases of UBS and SBS, Russian Roulette was turned off. SBS was run with a splitting field size parameter, FS of 30 cm. DBS was run with electron splitting and the splitting and Russian Roulette (RR) plane locations indicated in the figure. Note the single points indicating efficiency with DBS at NBRSPL$=1000$ with no Russian Roulette plane ("$\times$") and with a Russian Roulette plane but no charged particle splitting ("*").

1. Selecting the splitting number (NBRSPL)

Figure 2 shows the total photon fluence efficiency in the beam field vs bremsstrahlung splitting number (NBRSPL) for UBS, SBS, and DBS. Efficiencies have been normalized to the total photon fluence efficiency with no splitting. In the case of UBS and SBS, results are shown with Russian Roulette on (empty circles) and off (filled circles). SBS was run with a splitting field size, FS, parameter of 30 cm, which is the value used by Sheikh-Bagheri and Rogers[9,10] in their simulations of Elekta photon beams. Results for DBS are shown with no electron splitting (empty circles) and with electron splitting on with the splitting plane at $Z=15.46$ cm and the Russian Roulette plane at $Z=15.2$ cm. Results with electron splitting on and the splitting plane at $Z=15.66$ cm (the very bottom of the flattening filter) and the Russian Roulette plane at $Z=15.5$ cm are indistinguishable from the results shown. We therefore assume that the trend in photon fluence efficiency vs NBRSPL is independent of the placement of the splitting and Russian Roulette planes in DBS.

From Fig. 2 it is clear that DBS, with or without electron splitting, is a significant improvement over UBS and SBS. The maximum improvement in photon fluence efficiency using DBS (with NBRSPL$=2500$, no electron splitting) is a factor of 500, over 8 times the maximum efficiency using SBS (with NBRSPL$=2500$ and Russian Roulette on) and 20 times that achieved using UBS (with NBRSPL$=750$ and Russian Roulette on). For all splitting algorithms, the production of electrons (either by turning Russian Roulette off or by turning electron splitting on) results in a decrease in photon fluence efficiency by a factor of 3 and a shift of the splitting number (NBRSPL) at which the photon efficiency peaks toward lower values.

Since users are generally interested in electrons at the bottom of the accelerator, Fig. 2 suggests using a splitting number of 100 for peak photon efficiency in UBS. The original BEAM paper[1] suggests using NBRSPL values in the range 10–20, but at that time, when Russian Roulette was used, secondary fat electrons were not split as they are now. The previously suggested range would result in a photon efficiency well below the maximum and implies that the most recent implementation of UBS in BEAMnrc, which uses the built-in bremsstrahlung splitting function in EGSnrc,[7] is more efficient than UBS in older versions of BEAM (up to and including BEAM00).

In the case of SBS, Fig. 2 indicates that maximum photon efficiency is achieved with NBRSPL$=1000$. It is important to note that, in SBS, NBRSPL represents the maximum possible splitting number, and that the actual bremsstrahlung splitting number is a calculated value falling somewhere between the user-input minimum splitting number, NMIN (given its suggested value of NBRSPL/10 in all of these simulations), and NBRSPL. The BEAMnrc Manual[2] suggests a value of NBRSPL in the range 200–1000, which is certainly reasonable given that there is little variation in photon fluence efficiency over this range.

Figure 2 indicates the splitting number for maximum photon efficiency in DBS (with electron splitting) is 1000. Additional results with the electron splitting plane at $Z=15.66$ cm and the Russian Roulette plane at $Z=15.5$ cm indicate that this optimum value of NBRSPL does not change with the positions of the these planes. Positioning of the splitting and Russian Roulette planes will be discussed in more detail below.

The electron fluence efficiencies as a function of bremsstrahlung splitting number are shown in Fig. 3 relative to the total electron fluence efficiency with no splitting. To generate electrons with UBS and SBS, Russian Roulette was turned off. As in the plot of photon fluence efficiency vs NBRSPL, the splitting field size, FS, was set to 30 cm. In the case of DBS, electron splitting was turned on and two sets of splitting plane and Russian Roulette plane positions were used to demonstrate that the behavior of total electron fluence efficiency as a function of NBRSPL follows the same trend independent of the setting of these two parameters. Note that single points are shown for DBS (NBRSPL=1000) with a splitting plane (Z=15.66 cm) but no Russian Roulette plane and with a Russian Roulette plane (Z=14.9 cm) but no splitting plane.

Figure 3 shows that using DBS can result in 8 times greater electron fluence efficiency than SBS and 20 times greater efficiency than UBS. In the case of UBS and SBS, electron fluence efficiency shows little variation with NBRSPL over the range of splitting numbers studied. This means that the splitting number for maximum photon fluence efficiency (100 in the case of UBS and 1000 in the case of SBS) is adequate for electron efficiency as well. Directional bremsstrahlung splitting, on the other hand, has a definite maximum in electron fluence efficiency occurring at NBRSPL =1000. This is also the splitting number for maximum photon fluence efficiency when using DBS. The two DBS curves, each with different Z positions of the splitting and Russian Roulette planes, indicate that the placement of these planes has little effect on the behavior of electron fluence efficiency as a function of NBRSPL. The point with no Russian Roulette plane indicates that the Russian Roulette plane is essential for good electron statistics with DBS, with the addition of the Russian Roulette plane increasing electron fluence efficiency by a factor of almost 30 at NBRSPL =1000. Conversely, the point with no splitting plane illustrates that it is necessary to split fat charged particles. If they reach the field then they can decrease the efficiency by a factor of ≈80.

2. Selecting splitting field size (FS and splitting radius)

Another consideration when using SBS and DBS is selection of the splitting field size at the bottom of the accelerator. In SBS, the user is asked to input a field size parameter, FS, which the BEAMnrc Users Manual[2] suggests setting equal to the longest side of the treatment field plus 10 cm. In DBS, the user inputs a field radius which must include, as a minimum, the entire treatment field.

Figure 4 shows the relative efficiency when scoring total photon and electron fluence within the 10×10 cm^2 field of the SL25 6 MV photon beam as a function of FS for SBS and splitting field radius for DBS. Since we were interested in generating electrons, Russian Roulette was turned off in SBS, and electron splitting was turned on in DBS (Z of splitting plane=15.66 cm, Z of Russian Roulette plane =15.5 cm). The bremsstrahlung splitting number (NBRSPL) was set to 1000 for both SBS and DBS, since this was shown to give maximum photon fluence efficiency when electrons were generated (see Sec. IV B 1).

For SBS, Fig. 4 shows that photon fluence efficiency peaks at FS=40 cm, although there is little variation in efficiency beyond FS=30 cm. Electron fluence efficiency increases constantly over the range of FS values studied, but also shows little variation over a wide range of FS. Based on maximizing photon fluence efficiency, the setting of FS =30 cm used by Sheikh-Bagheri and Rogers[9,10] (and used elsewhere in this study) is certainly adequate, but the value of FS suggested by the BEAMnrc manual (treatment field size+10 cm=20 cm) is slightly low.

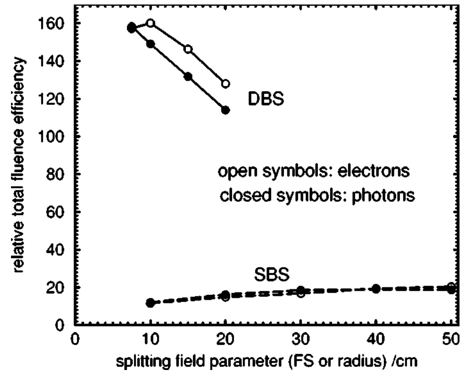

FIG. 4. Total photon (closed circles) and electron (open circles) fluence efficiency inside the 10×10 cm^2 field of the simulated Elekta SL25 6 MV photon beam versus the size of the bremsstrahlung splitting field [FS (width of a square field) for SBS and radius for DBS]. Efficiencies shown are relative to their counterparts with no splitting. SBS was run with Russian Roulette off and DBS was run with electron splitting on, with the splitting plane at Z=15.66 cm (the back of the flattening filter) and the Russian Roulette plane at Z=15.5 cm. The splitting number (NBRSPL) for both SBS and DBS was 1000, which was shown to give maximum photon fluence efficiency when electrons are generated.

In the case of DBS, Fig. 4 shows that photon fluence efficiency constantly decreases with increasing splitting field radius. This behavior is expected since increasing the splitting field size increases the number of events that must be split. Electron fluence efficiency, on the other hand, shows a peak at splitting radius=10 cm. From the point of view of maximizing photon fluence efficiency, it would seem that the optimum splitting radius would be the smallest that completely encompasses the 10×10 cm^2 treatment field (e.g., ≈7.1 cm). However in this particular accelerator, significant contributions to dose are made by photons out to a radius of 10 cm. Thus, we use a splitting radius of 10 cm for the rest of the study. This results in only a ≈6% drop in photon fluence efficiency compared to a splitting radius of 7.5 cm and also maximizes electron fluence efficiency.

3. Selecting position of splitting and Russian Roulette planes (DBS)

Further degrees of freedom are available in DBS for optimizing photon and electron fluence efficiency, *viz*., the setting of the positions of the electron splitting and Russian Roulette planes. The function of these planes is described in detail in Sec. III H. The splitting plane should be set close to the bottom of the flattening filter to maximize the number of electrons reaching the bottom of the accelerator while minimizing the time spent transporting them in such structures as the primary collimator and the flattening filter itself. The Russian Roulette plane, below which Russian Roulette is not played on electrons resulting from interactions and low-weight photons are allowed to interact, should be placed

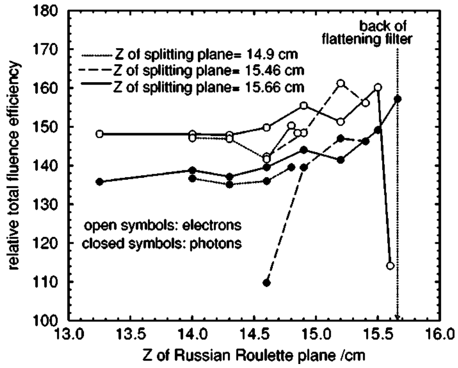

FIG. 5. Total photon (closed circles) and electron (open circles) fluence efficiency inside the 10×10 cm^2 field of the simulated Elekta SL25 6 MV photon beam versus the Z position of the Russian Roulette plane in DBS. Photon and electron efficiencies shown are relative to photon and electron efficiencies with no splitting. Curves are shown for three different Z positions of the electron splitting plane: 14.9 cm, 15.46 cm, and 15.66 cm. $Z=14.9$ cm and $Z=15.46$ cm correspond to layer boundaries in the modelled flattening filter, while $Z=15.66$ cm corresponds to the plane defining the bottom of the flattening filter. For these simulations, the splitting number was 1000 (shown to give maximum photon and electron fluence efficiency in DBS) and the splitting field radius was 10 cm.

above the splitting plane. Due to the way electron splitting is coded, the splitting plane is restricted to being coincident with a geometrical plane in the BEAMnrc component module in which it is located. Thus, in the flattening filter, this plane must coincide with a layer boundary in the modelled flattening filter or with the planes defining the top or bottom of the flattening filter. There is no such restriction on the position of the Russian Roulette plane.

Figure 5 shows the relative total photon and electron fluence efficiency inside the 10×10 cm^2 field of the simulated SL25 6 MV photon beam as a function of the position of the Russian Roulette plane. Curves are shown for splitting plane Z positions of 14.9 cm and 15.46 cm, both corresponding to layer boundaries in the modelled flattening filter, and for splitting plane $Z=15.66$ cm, corresponding to the bottom of the flattening filter. The Russian Roulette plane was always placed above the splitting plane. The splitting number (NBRSPL) was set to 1000 (shown above to maximize photon and electron fluence efficiency in DBS) and the splitting field radius was 10 cm.

The curves show that photon fluence efficiency increases as the splitting plane is brought closer to the Russian Roulette plane and also as both planes are brought closer to the bottom of the flattening filter (15.66 cm). Ignoring the outlier at splitting plane $Z=15.46$ cm and Russian Roulette plane $Z=14.6$ cm, the overall variation in photon fluence efficiency is $\approx16\%$ over the range of splitting and Russian Roulette plane positions studied. Note that, again not considering the outlying point, the photon efficiency for a given Russian Roulette plane position does not change appreciably with splitting plane position.

Electron fluence efficiency shows a similar trend to photon fluence efficiency with the exception that there is a drop off in efficiency once the splitting plane is very close to (within 0.06 cm of) the Russian Roulette plane. This is especially noticeable in the case with the Russian Roulette plane at $Z=15.66$ cm and the splitting plane at $Z=15.6$ cm. Ignoring this extreme point, though, the overall change in electron fluence efficiency is $\approx12\%$ over the range of plane positions studied.

Based on the above results, we selected a splitting plane position of $Z=15.66$ cm (i.e., at the base of the flattening filter) with the Russian Roulette plane at $Z=15.5$ cm. This results in near-maximum values of the photon and electron fluence efficiencies while not sacrificing one efficiency for the other (as done with splitting plane $Z=15.66$ cm and Russian Roulette plane $Z=15.6$ cm, or splitting plane $Z=15.46$ cm with Russian Roulette plane $Z=15.2$ cm). However, exact placement of these planes is not critical as long as they are near the back of the flattening filter, since the variation in both photon and electron fluence efficiencies with the positions of the splitting and Russian Roulette planes tends to be relatively small.

It is important to note that the curves shown in Fig. 5 are not general, and the behavior of photon and electron fluence efficiencies with splitting and Russian Roulette plane positions will most likely depend upon the flattening filter model and the beam energy.

C. Fluence efficiency profiles

Figure 6 shows the relative fluence efficiency for photons (a) and electrons (b) as a function of X at $Y=0$ at the SSD (100 cm) of the simulated SL25 6 MV photon beam. The splitting parameters used were those determined based on results in Sec. IV B above.

Photon fluence efficiency profiles are constant within the 10×10 cm^2 beam field (i.e., from $X=-5$ to 5 cm) with the relative efficiency approximately equal to the relative efficiency totalled over the entire beam field for the same splitting routine/parameters (see Sec. IV B above). Beyond the beam field the UBS efficiency profile remains constant at a factor of ≈7 times the efficiency with no splitting. This illustrates the main limitation of UBS, in which bremsstrahlung splitting is equal in all directions. In the case of SBS, selective bremsstrahlung splitting causes the photon fluence efficiency to drop by a factor of ≈2 beyond the edges of the field. Even so, the efficiency outside the field remains quite high due to the fact that, with FS=30 cm, the splitting field goes well beyond the edges of the field, and to the fact that even photons aimed beyond the edges of the splitting field are split by the background splitting number (NMIN). The DBS efficiency profile, on the other hand, falls off to very low values (≈0.3 times the efficiency with no splitting) beyond the edge of the splitting field ($r=10$ cm) since no splitting is done there. The large variations in the DBS efficiency profile between the edge of the field and the edge of the splitting field are due to the fact that the fluence with no splitting, used to normalize these profiles, has large uncertainties in this region.

In contrast to the photon fluence efficiency, electron fluence efficiency profiles [Fig. 6(b)] are almost constant over the entire range of X values for all splitting routines, with the

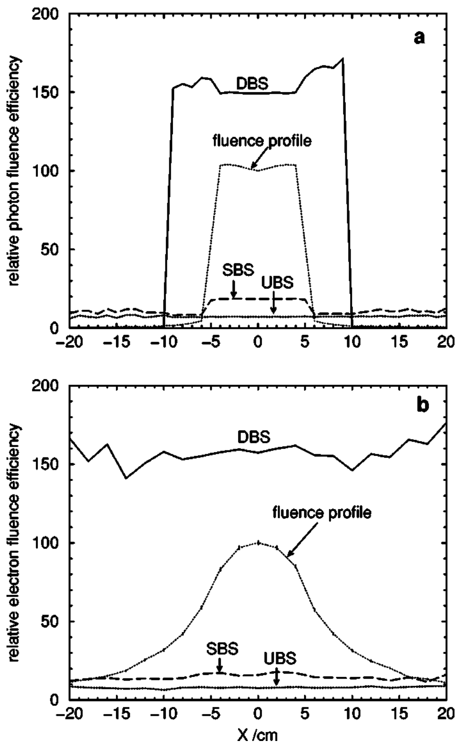

FIG. 6. Fluence efficiency for photons (a) and electrons (b) vs X at $Y=0$ at the SSD (100 cm) of the simulated Elekta SL25 6 MV photon beam (10×10 cm^2 field). Photon fluence was scored in 1×1 cm^2 zones, and electron fluence was scored in 2×4 cm^2 zones. Efficiencies are relative to their counterparts with no splitting. UBS was run with Russian Roulette off and NBRSPL=250. SBS was run with Russian Roulette off, NBRSPL=1000 and FS=30 cm. DBS was run with NBRSPL=1000, splitting field radius=10 cm, and electron splitting on with splitting plane $Z=15.66$ cm and Russian Roulette plane $Z=15.5$ cm. The photon and electron fluence profiles are also shown.

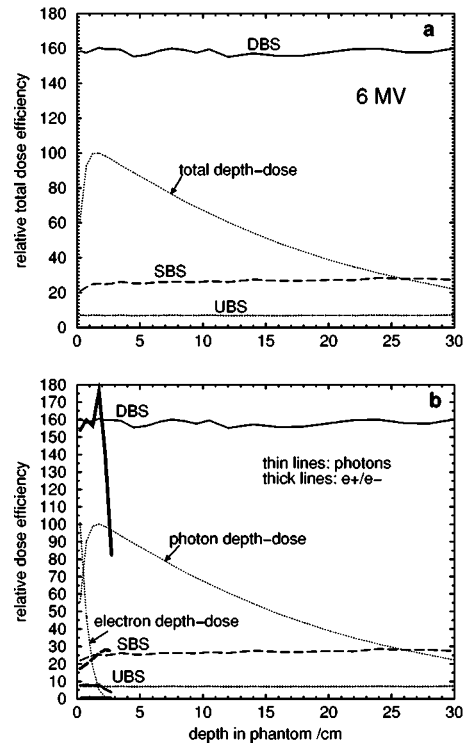

FIG. 7. Efficiency of central-axis dose as a function of depth in phantom for the simulated 6 MV SL25 photon beam (10×10 cm^2 field). Dose scoring volumes had radii 1 cm and thicknesses in the range 0.5–2 cm. Efficiencies have been normalized by the efficiency with no splitting. (a) shows total dose efficiency and (b) shows efficiency of dose contributions from photons and charged particles (thick lines) separately. Normalized depth-dose profiles are also shown for all cases. Splitting parameters are the same as in Fig. 6.

relative electron efficiency approximately equal to the relative electron efficiency totalled over the beam field in Sec. IV B for the same splitting routine/parameters.

D. Dose efficiency

Central-axis relative efficiencies for calculating dose as a function of depth in phantom for the simulated 6 MV beam using the splitting parameters optimized for photon and electron fluence efficiency are shown in Fig. 7. Figure 7(a) shows total dose efficiencies and Fig. 7(b) shows the efficiencies of the dose contributions of photons and electrons separately. Normalized depth-dose profiles are also shown in Fig. 7.

An inherent feature of the DBS technique is the occurrence of fat photons outside the splitting field radius. We have found that these fat photons can introduce a very large uncertainty in the dose in a phantom, despite the fact that these photons contribute a very small fraction of the dose in the beam. We have therefore added an option to our codes for scoring dose in a phantom (i.e., DOSXYZnrc and the CHAMBER CM in BEAMnrc) which allows us to ignore the dose from these fat photons. In the case of DBS in Fig. 7, contributions from fat photons that enter the phantom from outside the splitting field radius (10 cm) have been excluded. In separate calculations we have shown that these photons only contribute about 0.1% of the dose maximum to the dose in the phantom. At the same time they lead to large fluctuations in the efficiency of the dose calculation since a few photons carry so much weight. It is clear that the size of the contribution from excluded fat photons must be determined in each situation, to ensure they are not of importance. It may be necessary to increase the splitting field radius to ensure that their contribution to dose can be safely ignored and, thus, the efficiency of the dose calculation increased.

In the case of total dose efficiency, Fig. 7(a) shows that, for all splitting routines, the improvement in efficiency is essentially constant over all depths in the phantom. DBS resulted in the largest efficiency gain, with an improvement by a factor of 6 over SBS and an improvement by a factor of 23 over UBS. The photon dose efficiencies shown in Fig. 7(b) are almost indistinguishable from the total dose efficiencies, since the total dose is almost entirely comprised of photons. There is some contribution from electrons at the surface, however, and over the range of depths in which electron dose is significantly greater than zero (0–2.5 cm), the electron dose efficiency gain for a given splitting routine is similar to the photon dose efficiency gain. There are larger

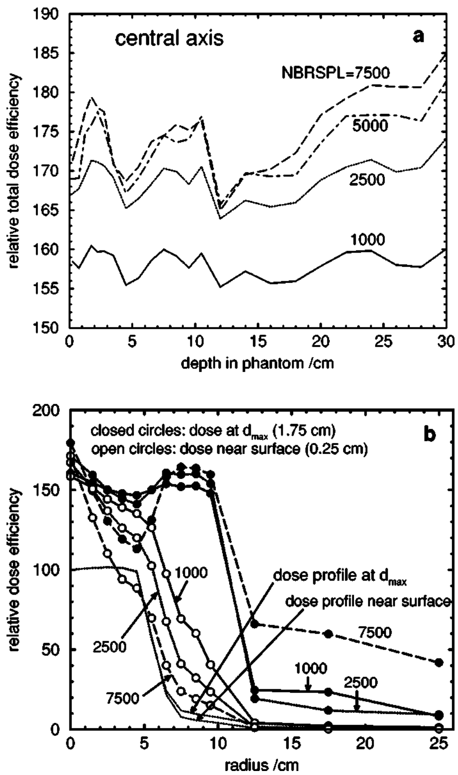

FIG. 8. Total dose efficiency vs depth (a) and vs radius (b) in phantom for the simulated 6 MV SL25 photon beam using DBS with different values of NBRSPL as indicated. Efficiencies have all been normalized to efficiencies with no splitting. In (b) the NBRSPL = 5000 results (dotted–dashed line) have been dropped to avoid confusion. Also in (b), efficiency vs radius results are shown at d_{max} (1.75 cm—closed circles) and near the surface of the phantom (0.25 cm depth—open circles). Other DBS parameters were the same as in Figs. 6 and 7.

variations in electron dose efficiency (especially visible in the case of DBS) since the uncertainties in electron dose are relatively high.

To confirm that optimizing parameters for fluence efficiency resulted in the maximum dose efficiency we also examined dose efficiency in the phantom while varying several of the splitting parameters in DBS. Of these parameters, only the splitting number, NBRSPL, had an effect on dose efficiency.

Figure 8 shows relative total dose efficiency in the phantom when using DBS with several different values of NBRSPL in the simulated 6 MV SL25 photon beam. Figure 8(a) shows the central axis dose efficiency, and Fig. 8(b) shows dose efficiency as a function of radius in the phantom at d_{max} (1.75 cm depth—closed circles) and near the surface of the phantom (0.25 cm depth—open circles). Normalized dose profiles at the two depths are also shown in Fig. 8(b) for reference. This figure emphasizes that the efficiency improvement depends strongly on exactly what quantity is of interest. Although our setting of NBRSPL = 1000 does not maximize dose efficiency on the central axis, it does maximize efficiency at all other radii near the surface (which is consistent with the fact that NBRSPL = 1000 resulted in maximum total fluence efficiency in the beam field) and also results in maximum or near-maximum efficiency at most radii at d_{max}.

TABLE I. CPU times required by simulated 6 MV photon beam from an Elekta SL25 accelerator (10×10 cm^2 field) using DBS with all possible combinations of the time-saving subroutines do_smart_brems and do_smart_compton. CPU times are relative to CPU time using both do_smart_brems and do_smart_compton. The top table shows results with electron splitting off, and the bottom table shows results with electron splitting on.

		do_smart_brems ON	do_smart_brems OFF
do_smart_compton	ON	1.0	5.3
	OFF	3.3	7.6

No electron splitting

		do_smart_brems ON	do_smart_brems OFF
do_smart_compton	ON	1.0	2.43
	OFF	1.77	3.2

Electron splitting with Z of splitting plane = 15.66 cm (back of the flattening filter) and Z of Russian Roulette plane = 15.5 cm

E. Performance of do_smart_brems and do_smart_compton

As mentioned in Secs. III A and III C above, DBS makes use of the subroutines do_smart_brems and do_smart_compton to eliminate the need for sampling and then playing Russian Roulette with split photons not aimed into the field by only generating those photons that will be aimed into the field. In order to determine how much CPU time these subroutines actually save, we have simulated the 6 MV SL25 photon beam using DBS (parameters optimized as described above) with all possible combinations of do_smart_brems and do_smart_compton turned on and off.

Results from this timing study are shown in Table I. The top table shows the results with electron splitting off and the bottom table shows results with electron splitting on. Note that in each table, the CPU times have been normalized to the time with both do_smart_compton and do_smart_brems on (i.e., the default case).

When electron splitting is off (upper Table I), it is clear that both of the smart subroutines contribute significantly to the high efficiency of DBS, with do_smart_brems playing a slightly larger role than do_smart_compton. This simply indicates that when the smart routines are not used, more time is spent simulating bremsstrahlung events than simulating Compton events. It is interesting to note that the increase by a factor of 7.6 in CPU time with both subroutines off is equal to the difference in photon fluence efficiency between SBS (with Russian Roulette on and NBRSPL = 1000) and DBS (with electron splitting off and NBRSPL = 1000) shown in Fig. 2.

When electron splitting is on (lower Table I), the contributions of both do_smart_brems and do_smart_compton to the efficiency of DBS decrease. This is due to the fact that a much larger portion of the time in this simulation is spent tracking electrons independent of the use of do_smart_brems or do_smart_compton. Interestingly, the contribution of do_smart_compton

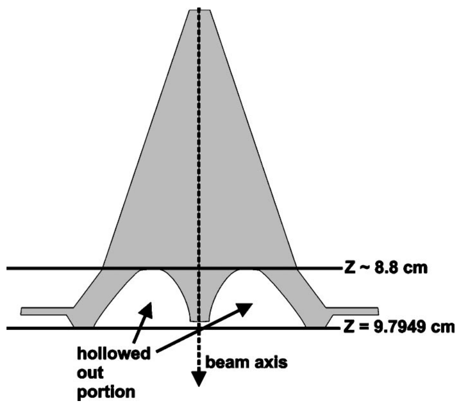

FIG. 9. Cross section through the flattening filter in the 18 MV KD2 photon beam showing the Z positions of the back of the flattening filter and the Z position where the hollowed out portion of the filter begins. The flattening filter is made of stainless steel.

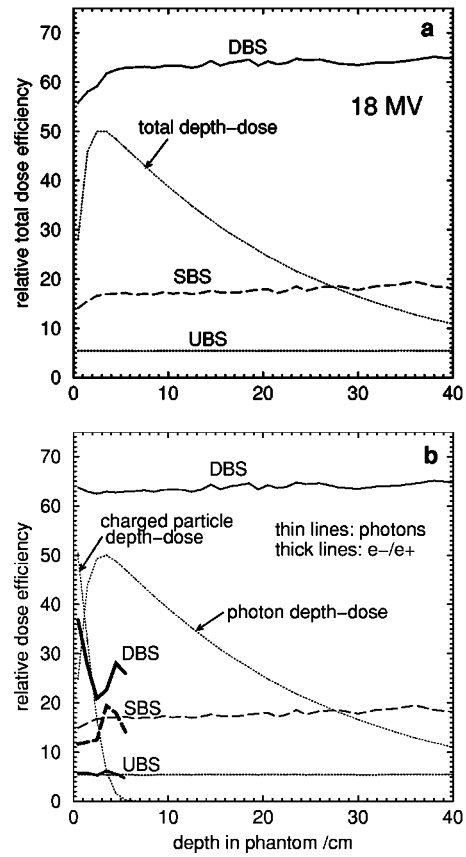

FIG. 10. Dose efficiency vs depth in phantom for a simulated 18 MV photon beam from a Siemens KD2 accelerator (10×10 cm^2 field). (a) shows total dose efficiency and (b) shows the efficiencies of the photon (thin lines) and charged particle (thick lines) components. Separately normalized depth-dose curves are shown for reference. For UBS, NBRSPL=250. For SBS, NBRSPL =1000 and FS=30 cm. DBS used NBRSPL, splitting radius=10 cm, electron splitting plane Z=9.795 cm (the back of the flattening filter) and Russian Roulette plane Z=9 cm. For DBS, total dose efficiency shown in (a) excludes fat photons.

relative to do_smart_brems is approximately the same as when electron splitting is turned off, yet electron splitting precludes the use of do_smart_compton below the Russian Roulette plane even when do_smart_compton is on. This indicates that the CPU time required for split Compton events below the Russian Roulette plane is completely overshadowed by the CPU time required for electron transport. Note that the factor of 3.2 increase in CPU time when both do_smart_compton and do_smart_brems are off is only a fraction of the factor of 8 difference in photon fluence efficiency between DBS (electron splitting on, NBRSPL=1000) and SBS (Russian Roulette off, NBRSPL=1000) shown in Fig. 2, underscoring the fact that these subroutines play less of a role in the efficiency of DBS when electrons are generated.

V. PERFORMANCE OF DBS AT HIGH ENERGY

To test the performance of DBS at a higher photon energy, we simulated an 18 MV photon beam (10×10 cm^2) field from a Siemens KD2 accelerator and examined central-axis dose in a phantom at the SSD (100 cm). Geometrical parameters were identical to those used by Sheikh-Bagheri and Rogers in their study of photon beams.[9,10] In addition to the various bremsstrahlung splitting routines (parameters discussed in more detail below), charged particle range rejection was used, with ESAVE=5 MeV, in all simulations.

In the case of UBS and SBS, the splitting parameters (NBRSPL and, for SBS, the splitting field size, FS) found to optimize fluence or dose efficiency in the simulated SL25 6 MV photon beam above were also found to optimize dose efficiencies in the KD2 18 MV simulation. Thus, for UBS NBRSPL was set to 250, and for SBS NBRSPL was set to 1000 and FS was set to 30 cm. In the case of DBS, the positions of the electron splitting and Russian Roulette planes had to be changed to reflect the geometry and position of the flattening filter in the KD2 18 MV accelerator. As in the SL25 accelerator, the highest efficiencies were obtained with the splitting plane placed right on the bottom surface of the flattening filter (Z=9.8 cm). However, some trade-offs were involved in placement of the Russian Roulette plane due to the shape of the flattening filter in the KD2. The flattening filter of the KD2 has a hollowed out portion near the bottom (see Fig. 9). When the Russian Roulette plane was placed slightly above this portion (at Z=8.7 cm), the efficiency gain obtained using DBS was approximately equal for both the photon and charged particle components of the dose. However, when the Z position of the Russian Roulette plane was increased to 9 cm (now cutting through the hollowed out portion of the flattening filter), the efficiency of the photon portion of the dose increased by 45%, while the efficiency of the charged particle portion decreased by up to 40%. Since the photon portion of the dose dominates the total dose at every depth, with the charged particle portion only making significant contributions in the first 5 cm of depth, we opted for the lower (Z=9 cm) placement of the Russian Roulette plane. In addition, the bremsstrahlung splitting number of 1000 found to optimize dose efficiency at 6 MV in the SL25 accelerator did not optimize central-axis dose efficiency in the KD2. By decreasing NBRSPL to 750, we were able to obtain a 14% increase in efficiency over that obtained with NBRSPL =1000.

Figure 10 shows the dose efficiencies on the central axis of the phantom (voxel radius = 1 cm, voxel thickness = 1 cm or 2 cm) placed at SSD = 100 cm in the 18 MV KD2 photon beam using the splitting parameters discussed above. The total dose efficiency shown in Fig. 10(a) is broken down into the efficiencies of the photon and charged particle components in Fig. 10(b). The corresponding depth-dose curves are also shown for reference. All efficiencies are relative to efficiency with no splitting. Efficiencies for the DBS case do not include any fat photons.

Figure 10(a) shows that DBS increased the efficiency in dose calculations on the central axis by a factor of 3.6 over SBS and by a factor of 13 over UBS. Although still offering substantial improvement over the other splitting routines, efficiency with DBS relative to no splitting dropped by a factor 2.5 from its performance in the 6 MV SL25 beam. By comparison, relative efficiency with SBS is a factor of 1.5 lower than in the 6 MV case, and UBS drops by a factor of only 1.3. One reason for the relative decrease in efficiency of SBS and DBS is that at higher energies the angular distribution of bremsstrahlung and Compton scattered photons becomes more forward peaked. In the case of SBS, this means that the splitting number will be very high for photons directed into the splitting field. For DBS, the implication is that fewer photons can be eliminated as being aimed away from the splitting field.

Another way to look at these results is to note that the overall efficiency of the BEAMnrc calculation with no splitting increases by a factor of about 2.7 going from 6 MV to 18 MV. This is because of the more forward peaked photons at the higher energy. This means that the overall efficiency of the DBS algorithm does not change much between the 6 MV and 18 MV cases because it has been optimized for the forward-going photons.

In addition, the total dose efficiency with both SBS and DBS drops off near the surface of the phantom. Figure 10(b) shows that this drop-off is due to the lower efficiency in the charged particle contribution to the dose relative to the efficiency of the photon component of the dose in the case of DBS and SBS (charged particles account for 12.5% of the total dose near the surface of the phantom). The reason for the lower charged particle dose efficiency in the case of DBS (a factor of up to 3 lower than the efficiency of the photon component) has been discussed above, in which we opted for a placement of the Russian Roulette plane that would optimize the photon dose efficiency at the expense of some charged particle efficiency.

VI. PERFORMANCE OF DBS IN A BROAD BEAM

We also tested the performance of DBS in the simulated 6 MV SL25 photon beam by examining fluence efficiency at the SSD (100 cm) with the jaws widened to give a 40×40 cm^2 field. The jaws simulated in this case were the "standard" jaws (10 cm thick, comprising 5 cm of tungsten and 5 cm of lead) instead of the jaws for use with a multileaf collimator that were used to determine performance of DBS with a 10×10 cm^2 field in this accelerator (see Sec. IV above). Other than the jaws and their settings, the simulation geometry and other parameters were identical to those used with the 10×10 cm^2 field.

The splitting parameters used for all splitting routines were those found to optimize performance in the 6 MV SL25 accelerator with a 10×10 cm^2 field (see Sec. IV B above), with the exception of the splitting field size, FS, in SBS and the splitting field radius in DBS. For SBS, FS was set to 60 cm. This setting is based on the performance of SBS as a function of FS in the 10×10 cm^2 beam (see Sec. IV B 2 above), where little improvement in photon fluence efficiency was observed for values of FS > field size + 20 cm. The splitting radius used in DBS was 30 cm. This radius completely encloses the 40×40 cm^2 field, allowing for 2 cm beyond the corners of the field. Note that with such a large splitting radius, the difference in efficiency with a small change in the splitting radius (e.g., reducing it by 2 cm so that it exactly encloses the field) is expected to be negligible.

For the purposes of scoring fluence, the phase-space surface at SSD = 100 cm was divided into 6561 (81×81) 1×1 cm^2 scoring zones. As with the study of photon fluence efficiency in the 10×10 cm^2 beam, efficiency of all splitting algorithms is expected to increase as the area of the scoring zones is decreased (see Sec. IV A above). Unlike the 10×10 cm^2 field case, the 1×1 cm^2 scoring zones were used for both photon and electron fluence efficiency profiles.

Figure 11 shows the photon (a) and electron (b) fluence efficiency profiles (efficiency vs X at $Y=0$) at SSD = 100 cm in the 40×40 cm^2 beam. Efficiencies are relative to efficiency with no splitting. Photon and electron fluence profiles are also shown for reference. The fluctuations in relative electron fluence efficiency with DBS visible in Fig. 11(b) are due mainly to fluctuations in efficiency with no splitting (i.e., the normalizing quantity) ultimately caused by the small scoring zones.

It is clear from the figures that, in the broad beam, DBS still offers a substantial improvement in efficiency over the other splitting routines. In the case of photon fluence within the field (-20 cm $\leqslant X \leqslant 20$ cm), DBS is between 5.5 (at the center of the field) and 7 (at the edges of the field) times more efficient than SBS and is ≈ 12 times more efficient than UBS. Between the edges of the field and the edge of the splitting field (20 cm $\leqslant |X| \leqslant$ 30 cm), the relative photon efficiency with DBS increases, resulting in the "horns" in Fig. 11(a). This increase is due to the high uncertainty (low efficiency) in the photon fluence with no splitting in this region. In the case of electron fluence, the efficiency using DBS is ≈ 8 times greater than with SBS and ≈ 14 times greater than with UBS in the field.

The efficiency of DBS in the broad beam is significantly lower than in the 10×10 cm^2 beam (Fig. 6), with photon fluence efficiency inside the field dropping by a factor of ≈ 1.7 and electron fluence efficiency inside the field dropping by a similar amount. In comparison, photon fluence efficiency inside the field using SBS drops by a factor of only 1.1 (at the center of the field) to 1.5 (at the edges of the field) in the broad beam, with electron fluence efficiency dropping

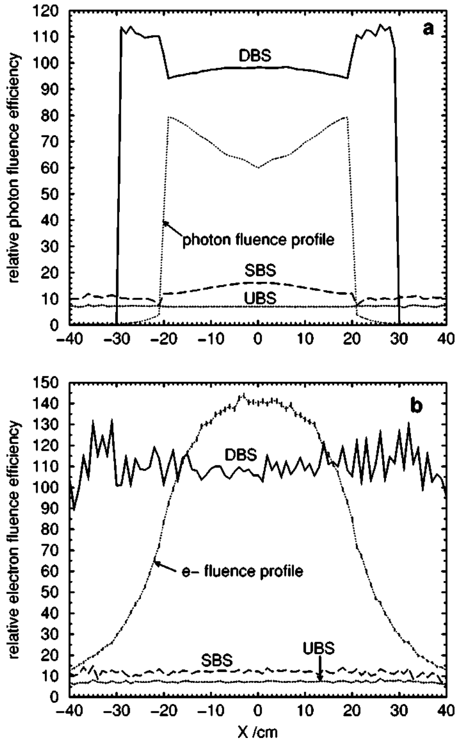

FIG. 11. Photon (a) and electron (b) fluence efficiency vs X (at $Y=0$) at the SSD (100 cm) for a simulated 6 MV SL25 photon beam with jaws expanded to give a 40×40 cm^2 field. Efficiencies are relative to the efficiency with no splitting. The arbitrarily normalized photon and electron fluence profiles at $Y=0$ are also shown for comparison. For UBS, NBRSPL was set to 250. For SBS, NBRSPL=1000 and the splitting field size, FS, was set to 60 cm. For DBS, NBRSPL=1000, splitting field radius was 30 cm, Z of the electron splitting plane was 15.66 cm (the back of the flattening filter), and Z of the Russian Roulette plane was 15.5 cm.

by a factor of only ≈1.2. In the case of UBS, the drop in photon and electron fluence efficiency in the broad beam compared to the 10×10 cm^2 beam is insignificant.

The directional splitting routines (SBS and DBS) are less efficient in the broad beam simply because of the required increase in splitting field size. In the case of DBS, this results in both fewer photons being eliminated by Russian Roulette and more photons being generated by the do_smart_brems and do_smart_compton subroutines. In the case of SBS, this results in a higher splitting number over a greater range of incident electron directions/energies. The reason that the overall efficiency drop in the broad beam is relatively greater for DBS than for SBS may be due to the increased number of split Compton interactions in DBS (SBS does not split these interactions). In the case of UBS, the change in field size does not change the number of split photons that must be tracked, resulting in no significant efficiency change.

It is interesting to note that for a given splitting routine in both broad beam and 10×10 cm^2 cases, the relative electron fluence efficiency is of the same order as the relative photon fluence efficiency which is useful since electron contamination plays a more important role in the broad beams.

VII. CONCLUSIONS

We have demonstrated that directional bremsstrahlung splitting (DBS) offers a significant improvement in photon and electron fluence and dose efficiency over the previously available bremsstrahlung splitting routines in BEAMnrc, uniform bremsstrahlung splitting (UBS) and selective bremsstrahlung splitting (SBS). In a "realistic" simulation of a 6 MV photon beam from an Elekta SL25 accelerator (10×10 cm^2 field) in which photons and electrons were generated (generation of electrons entailed turning Russian Roulette off in UBS and SBS and using electron splitting in DBS), the photon fluence efficiency inside the field when using DBS was a factor of 8 higher than when using SBS. Electron fluence efficiency in the field was a factor of almost 9 higher with DBS than with SBS. Efficiency of central-axis depth-dose in a phantom placed at the SSD (100 cm) was over 6 times higher with DBS than with SBS.

Obtaining the optimum efficiency gain with DBS required us to optimize settings of the bremsstrahlung splitting number, NBRSPL, the splitting field radius, and the positions of the electron splitting plane and Russian Roulette plane. For the 6 MV photon beam, we found that NBRSPL=1000 optimized the photon and electron fluence efficiency in the field. Since photon fluence efficiency decreased with increasing splitting field radius, it was important to choose the smallest radius that completely enclosed the field with some overlap to ensure that the contribution to central-axis dose from fat photons (photons coming back to the central axis from beyond the edge of the splitting field) was negligible. We found that a splitting field radius of 10 cm was sufficient to meet these requirements. Another consideration was the positions of the electron splitting and Russian Roulette planes. For a fixed splitting plane location, the efficiency could be varied by up to 10% by moving the Russian Roulette plane (Russian Roulette plane always above the splitting plane), with a trend towards higher efficiencies as both the splitting plane and Russian Roulette plane were brought closer to the bottom of the flattening filter.

The optimal settings for NBRSPL, splitting field radius and splitting and Russian Roulette plane positions will depend on the details of the accelerator being simulated. For example, the optimal setting of NBRSPL in our simulations of an 18 MV photon beam from a Siemens KD2 accelerator was 750. Also, the hollowed out portion of the flattening filter in this accelerator was a consideration in the optimal placement of the Russian Roulette plane in relation to the electron splitting plane. However, we can generalize and say that setting NBRSPL≃1000 will result in near-optimum performance, with adjustments around this number possibly increasing efficiency by 15%. It is also a general rule that the electron splitting plane should be placed at the back of the flattening filter with the Russian Roulette plane in a solid portion of the flattening filter somewhere above the splitting plane.

The fluence or dose efficiency improvement of DBS is also dependent on the particular accelerator being simulated, with relative efficiency improvements tending to decrease at higher photon energies. This is because the inherent efficiency of these simulations is higher since bremsstrahlung photons at higher energies are more forward-directed, so fewer are subject to Russian Roulette by the DBS splitting routine. In this study, we have shown that the improvement in central-axis dose efficiency that DBS has over SBS drops from a factor of 6 in the 6 MV SL25 accelerator to a factor of 3.6 in the 18 MV KD2 accelerator.

The relative efficiency of DBS also decreases with increasing field size. When the field size of the 6 MV SL25 photon beam was increased to 40×40 cm^2 (broad beam), the photon and electron fluence efficiencies in the field with DBS decreased by a factor of $\approx$1.7 from their values in the 10×10 cm^2 beam. This compared to a drop in SBS efficiency by a factor of 1.1 (center of field) to 1.5 (edges of field) for photon fluence and by a factor of $\approx$1.2 for electron fluence. Both SBS and DBS efficiencies were expected to drop due to the greater number of split photons that must be tracked in the broad beam, but the relatively greater efficiency decrease in DBS efficiency may be due to the greater number of split Compton events in the broad beam. Even so, DBS is still significantly more efficient than SBS in the broad beam, with photon fluence efficiency (inside the field) between 5.5 and 7 times greater than with SBS ($\approx$12 times greater than with UBS), and electron fluence efficiency $\approx$8 times greater than with SBS ($\approx$12 times greater than with UBS).

Overall, the efficiency improvement of DBS is substantial and it will save large amounts of CPU time in the simulation of photon beams.

ACKNOWLEDGMENTS

The authors acknowledge Daryoush Sheikh-Bagheri's contribution of the SBS algorithm in BEAMnrc and thank Michel Proulx for his continued support of the IRS computing cluster.

APPENDIX A: DO_SMART_BREMS ALGORITHM

Consider an electron (or positron) at position $\vec{x}=(x,y,z)$ travelling along the direction $\vec{u}=(u,v,w)$ that is about to undergo a bremsstrahlung event. The process is in a coordinate system where the beam axis is along the z axis and the upper plane of the photon target is at $z=0$. The circle of interest (COI, also denoted as field of interest in the main text) is in a plane perpendicular to the z axis and located at $\vec{x}_0=(0,0,d)$ (d is typically 100 cm) and has a radius of R (see Fig. 12). We assume that the angular distribution $p(\mu,\phi)$ of bremsstrahlung photons is described by the leading term of Eq. 2BS from the article by Koch and Motz:[12]

$$p(\mu,\phi)=\frac{1-\beta^2}{4\pi}\frac{1}{(1-\beta\mu)^2}. \tag{A1}$$

Here, μ is the cosine of the polar scattering angle [i.e., $\cos(\theta)$], ϕ is the azimuthal angle and β is the electron velocity in units of the speed of light. The probability given in Eq. (A1) is normalized over all angles to unity. The goal is to calculate the probability W that this electron will emit a bremsstrahlung photon that is pointed towards the circle of interest. If W is known and one wants to perform bremsstrahlung splitting with a splitting number of N, keeping only photons going towards the COI, only WN photons need to be

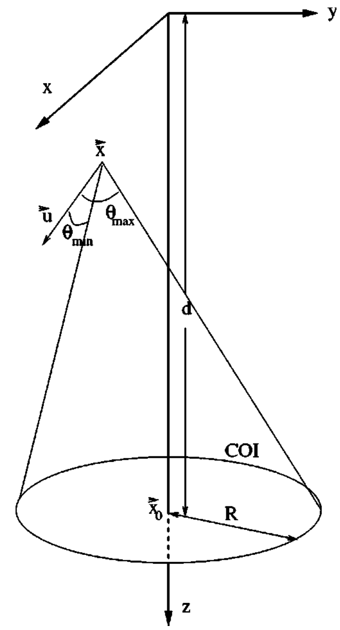

FIG. 12. The geometry used to derive the equations in Appendix A and B. Note that $\mu_{max}=\cos(\theta_{max})$, etc.

sampled provided that their angles are sampled so that they are directed towards the COI. If $W\ll 1$, a substantial saving of CPU time may be achieved.

The probability W is given by

$$W=\int_\Omega \mathrm{d}\mu\ \mathrm{d}\phi\ p(\mu,\phi), \tag{A2}$$

where the integration is to be carried out for all μ,ϕ within the solid angle Ω that result in a direction towards the COI. With the definitions

$$\begin{aligned} r &= \sqrt{x^2+y^2},\\ a_\pm &= \vec{u}(\vec{x}_0-\vec{x}) \pm R\sqrt{1-w^2},\\ t_{max} &= \sqrt{d^2+(R+r)^2},\\ t_{min} &= \begin{cases}\sqrt{d^2+(R-r)^2}, & r\leqslant R,\\ d, & r>R,\end{cases}\end{aligned} \tag{A3}$$

and simple geometrical considerations it is easy to see that the minimum and maximum polar scattering angles, μ_{min} and μ_{max}, that may result in a direction towards the COI are given by

$$\begin{aligned}\mu_{max} &= \mathrm{Min}(1,\mu_+), \quad \mu_+ = \begin{cases} a_+/t_{min}, & a_+\geqslant 0,\\ a_+/t_{max}, & a_+<0,\end{cases}\\ \mu_{min} &= \mathrm{Max}(-1,\mu_-), \quad \mu_- = \begin{cases} a_-/t_{max}, & a_-\geqslant 0,\\ a_-/t_{min}, & a_-<0.\end{cases}\end{aligned} \tag{A4}$$

The possible range of azimuthal scattering angles depends on $\vec{x}$, $\vec{x}_0$, and $\vec{u}$ in a complicated way. In addition, if the fact is taken into account that not all azimuthal angles will lead to a direction towards the COI, the integration in Eq. (A2) cannot be performed analytically. However, we can provide an upper limit of the probability W, denoted by W', by using all azimuthal angles. The correct number of photons towards the COI will result by simulating $W'N$ bremsstrahlung events and then rejecting photons not going towards the COI. We have

$$W' = 2\pi\int_{\mu_{\min}}^{\mu_{\max}} \mathrm{d}\mu\ p(\mu) = \frac{(1-\beta^2)(\mu_{\max}-\mu_{\min})}{2(1-\beta\mu_{\max})(1-\beta\mu_{\min})} \quad \text{(A5)}$$

with $\mu_{\min}$ and $\mu_{\max}$ defined via Eqs. (A3) and (A4).

The algorithm of the do_smart_brems subroutine is then as follows.

(1) Calculate $\mu_{\min}$, $\mu_{\max}$ and the estimated probability W'.
(2) Determine the number of photon angles, N', to be sampled. If we denote by $[\alpha]$ the integer part of α and by η a random number uniformly distributed between zero and unity, then $N'=[W'N]+1$, if $\eta \leqslant W'N-[W'N]$, $N'=[W'N]$, otherwise.
(3) Sample N' polar angles μ_i between $\mu_{\min}$ and $\mu_{\max}$ from the probability distribution $p(\mu)$ and azimuthal angles uniformly between 0 and 2π. Sampling μ_i is accomplished using

$$\mu_i = \frac{\mu_{\min}(1-\beta\mu_{\max})+\eta_i(\mu_{\max}-\mu_{\min})}{1-\beta\mu_{\max}+\beta\eta_i(\mu_{\max}-\mu_{\min})}, \quad \text{(A6)}$$

where η_i is a random number uniformly distributed between zero and unity.
(4) Reject all photons that do not go towards the COI. This will lead to a smaller number of photons N'', all of them having a weight of $1/N$.
(5) Sample a polar angle from $p(\mu)$ between -1 and 1. If this angle is not between $\mu_{\min}$ and $\mu_{\max}$, keep this photon with a weight of 1 and increase N'' by one.
(6) Sample N'' photon energies from the bremsstrahlung cross section differential in energy. If $N''=0$, sample one photon energy.
(7) Decrease the electron energy by the energy of the last sampled photon energy.

APPENDIX B: DO_SMART_COMPT ALGORITHM

Consider a photon with energy k, position $\vec{x}$ and direction $\vec{u}$ that is about to undergo a Compton scattering event modelled using the Klein–Nishina cross section.[13] Within the Klein–Nishina approximation each polar scattering angle $\mu=\cos(\theta)$ uniquely corresponds to a scattered photon energy k',

$$k' = \frac{k}{1+k(1-\mu)}, \quad \text{(B1)}$$

where for the simplicity of the notation all energies are expressed in terms of the electron rest energy. As discussed in Appendix A, the minimum and maximum angles, $\mu_{\min}$ and $\mu_{\max}$, that may result in a scattered photon going towards the circle of interest (COI) are given by Eq. (A4). The corresponding minimum and maximum scattered photon energies, $k'_{\min}$ and $k'_{\max}$ are given by Eq. (B1) with $\mu=\mu_{\min}$ or $\mu=\mu_{\max}$, respectively. The upper bound of the probability W for having the scattered photon moving towards the COI, W' (see Appendix A for discussion of why we must use W' instead of W), is

$$W' = \frac{\int_{k'_{\min}}^{k'_{\max}} \mathrm{d}k'\ \mathrm{d}\sigma_{\mathrm{KN}}/\mathrm{d}k'}{\int_{k/(1+2k)}^{1} \mathrm{d}k'\ \mathrm{d}\sigma_{\mathrm{KN}}/\mathrm{d}k'} = \frac{H(k_{\min},k_{\max})}{H(1/(1+2k),1)}, \quad \text{(B2)}$$

where $\mathrm{d}\sigma_{\mathrm{KN}}/\mathrm{d}k'$ is the Klein–Nishina cross section and

$$H(x_1,x_2) = \ln\frac{x_2}{x_1}(k^2-2k-2) + (x_2-x_1)\left(\frac{k}{x_1x_2}+\frac{1+2k}{k}+\frac{k}{2}(x_1+x_2)\right). \quad \text{(B3)}$$

The algorithm of the do_smart_compt subroutine is then as follows:

(1) Calculate $\mu_{\min}$, $\mu_{\max}$ and the probability W'.
(2) Determine the number N' of Compton interactions to be sampled. If we denote by $[\alpha]$ the integer part of α and by η a random number uniformly distributed between zero and unity, then $N'=[W'N]+1$, if $\eta \leqslant W'N-[W'N]$, $N'=[W'N]$, otherwise.
(3) Sample N' scattered photon energies between $k'_{\min}$ and $k'_{\max}$ from the Klein–Nishina cross section. The algorithm is very similar to the one used to sample the full distribution (see, e.g., the EGSnrc Manual[7]), except that the constants α_1 and α_2 have to be calculated using $k'_{\min}$ and $k'_{\max}$ instead of $k/(1+2k)$ and k as the integration limits.
(4) Calculate the corresponding scattering angles and photon directions and reject all photons not moving towards the COI. Also reject all electrons.
(5) Sample one Compton interaction without restrictions. Keep the resulting electron with a weight of 1. Keep the scattered photon only if its energy is not between $k'_{\min}$ and $k'_{\max}$ and give it the weight of 1.

[a]Present address: Physics Department, Carleton University, Ottawa K1S 5B6, Canada.
[b]Electronic mail: bwalters@irs.phy.nrc.ca

[1]D. W. O. Rogers, B. A. Faddegon, G. X. Ding, C.-M. Ma, J. Wei, and T. R. Mackie, "BEAM: A Monte Carlo code to simulate radiotherapy treatment units," Med. Phys. **22**, 503–524 (1995).
[2]D. W. O. Rogers, C.-M. Ma, G. X. Ding, B. Walters, D. Sheikh-Bagheri, and G. G. Zhang, BEAMnrc Users Manual, NRC Report PIRS 509(a)revF (2001).
[3]D. W. O. Rogers, Publications using or about BEAM or the OMEGA project, http://www.irs.inms.nrc.ca/inms/irs/BEAM/bibliog/omega_pubs.html
[4]D. W. O. Rogers, C.-M. Ma, G. X. Ding, B. Walters, D. Sheikh-Bagheri, and G. G. Zhang, BEAM98 Users Manual, NRC Report PIRS 509(a)revC (1998).
[5]D. Sheikh-Bagheri, "Monte Carlo study of photon beams from medical linear accelerators; optimization, benchmark and spectra," PhD thesis, Carleton University, Ottawa, 1999.
[6]I. Kawrakow, "Accurate condensed history Monte Carlo simulation of

electron transport. I. EGSnrc, the new EGS4 version," Med. Phys. **27**, 485–498 (2000).
[7]I. Kawrakow and D. W. O. Rogers, The EGSnrc Code System: Monte Carlo simulation of electron and photon transport, Technical Report PIRS–701, National Research Council of Canada, Ottawa, Canada, 2000.
[8]I. Lux and L. Koblinger, *Monte Carlo Particle Transport Methods: Neutron and Photon Calculations* (CRC Press, New York, 1991).
[9]D. Sheikh-Bagheri and D. W. O. Rogers, "Sensitivity of megavoltage photon beam Monte Carlo simulations to electron beam parameters," Med. Phys. **29**, 379–390 (2002).
[10]D. Sheikh-Bagheri and D. W. O. Rogers, "Calculation of nine megavoltage photon beam spectra using the BEAM Monte Carlo code," Med. Phys. **29**, 391–402 (2002).
[11]B. R. B. Walters, I. Kawrakow, and D. W. O. Rogers, "History by history statistical estimators in the BEAM code system," Med. Phys. **29**, 2745–2752 (2002).
[12]H. W. Koch and J. W. Motz, "Bremsstrahlung cross-section formulas and related data," Rev. Mod. Phys. **31**, 920–955 (1959).
[13]O. Klein and Y. Nishina, "Über die Streuung von Strahlung durch freie Elektronen nach der neuen relativistischen Quantendynamik von Dirac," Z. Phys. **52**, 853–868 (1929).